

Optimizing the Relative Contribution of Preparatory and Triggering Factors in Landslide Analysis System with an Eight-year Landslide Inventory - Validation with typhoon events and operation with real-time precipitation -

Cheng-Chien LIU,^{1,2,*} Mei-Chen CHEN,³ Yi-Ting LIN,² Sheng-Feng ZENG,³ Hui-Lin WEN,² Hsiao-Yuan YIN,³ En-Ju LIN,¹ and Nguyen Thi To NGAN

¹ Dept. of Earth Sciences, National Cheng-Kung University (Tainan 701, Taiwan ROC)

² Global Earth Observation and Data Analysis Center, National Cheng-Kung University (Tainan 701, Taiwan ROC)

³ Debris Flow Disaster Prevention Center, Soil and Water Conservation Bureau, Council of Agriculture (Nantou, Taiwan ROC)

*Corresponding author. E-mail: ccliu88@mail.ncku.edu.tw

Taiwan is the place on Earth most vulnerable to natural hazards, particularly the disasters of landslide that pose direct threat to human lives and cause enormous damage to properties. To manage and mitigate the catastrophic disaster caused by landslides is one of the most important tasks to be endeavored and addressed by Taiwan government. Based on the probabilistic approach of landslide analysis, we propose six strategies to develop a landslide analysis system (LAS), including prepare a long-term and detailed landslide inventory, select preparatory factors, establish a model of landslide susceptibility index (LSI), determine the weight of each preparatory factor, calculate landslide hazard index (LHI) using triggering factor, and evaluate the performance of model with actual events of landslide. The ultimate goal is to provide early warnings to the general publics and reduce the risk of slope hazards. With this new LAS, we revisit the event of debris flow occurred in He-Jung Village in 2012, and use the archive of QPESUM data to make a series of three-hour nowcasts. Comparing the LHI calculated by LAS to the actual sites of new landslides triggered in this event, the accuracy is as high as 69%. The possible sources of error and the room of further improvement are discussed. The future plan to provide nationwide nowcasts of landslide using this new LAS is also included.

Key words: preparatory factor, triggering factor, landslide susceptibility index, landslide hazard index, landslide inventory

1. INTRODUCTION

Taiwan is the place on Earth most vulnerable to natural hazards. According to a recent survey funded by World Bank, more than 90 percent of Taiwan's populations live in areas at high relative risk of death from earthquake, typhoon and slope hazards [Dilley *et al.*, 2005]. As more extreme weather events are attributed to the intensifying trend of global warming, the natural environment of Taiwan has been undergoing dramatic changes as well. It is observed that the frequency and scale of natural disasters are getting severe in Taiwan, particularly in the past few years. Among various disasters, landslides are destructive and rapid geological processes that pose

direct threat to human lives and cause enormous damage to settlements, roads, infrastructure, and other valuable resources [Domakinis *et al.*, 2008; Huang *et al.*, 2007]. To manage and mitigate the catastrophic disaster caused by landslides, therefore, is one of the most important tasks to be endeavored and addressed by Taiwan government.

As a matter of fact, many efforts have already been made by Taiwan government over the past few decades to collect all sorts of geospatial data. Four of them are directly related to landslide analysis:

- (a) Formosat-2, the first high-spatial-resolution satellite operated in a daily-revisit orbit, was successfully launched in May 2004 [C-C Liu, 2006]. It serves as

an ideal source of data to prepare a long-term and detailed landslide inventory, which plays the key role in determining the weight of each preparatory factor for landslide analysis.

- (b) Quantitative Precipitation Estimation and Segregation Using Multiple Sensor (QPESUMS) is a system that employs data of radar, satellite and rain gauge to improve the technology of estimating rainfall pattern and precipitation intensity. The real-time estimation and up to 72 hours forecast of nationwide precipitation are updated every ten minutes at a spatial resolution of 1.3km. It provides the crucial information of triggering factor for landslide analysis.
- (c) Airborne Light Detection and Ranging (LiDAR) uses light in the form of a pulsed laser to generate precise, three-dimensional information about the shape of the Earth and its surface characteristics. After the devastation of Typhoon Morakot in 2009, the significance of high-precision digital elevation model (DEM) was well-recognized. The airborne LiDAR was systematically employed to map Taiwan in three years of time, resulting in a high-precision DEM with one-meter resolution. It serves as a fundamental yet crucial source of data to derive preparatory factors for landslide analysis, such as slope and aspect.
- (d) Geological map is the outcome of field works that geologists acquire after a series of geology, mining or engineering geology surveys. The first geological map of Taiwan (scale: 1/300,000) was published in 1953, and two more editions (scale: 1/250,000 and scale: 1/500,000) in 1975. The later one was revised in 1986. The Central Geological Survey of Taiwan is in charge of the task to update the geological map of Taiwan to the scale of 1/50,000. It serves as another crucial source of data to provide preparatory factors for landslide analysis, such as geological composition (GC).

From the point of view of management and mitigation, it is preferable to integrate these valuable data into an operational model to analyse landslide susceptibility and hazard, with an ultimate goal of providing early warnings to the general publics to reduce the risk of slope hazards.

Aleotti and Chowdhury [1999] made a comprehensive review of landslide susceptibility and hazard analysis. They categorized various models into the deterministic approach and the probabilistic approach: the former calculates the limit-equilibrium of a point based on the infinite-slope model; while the later develops the probability functions based on landslide inventory. The deterministic approach in theory would be more accurate than the probabilistic approach. But when putting it into practice, a lot of parameters, such as lateral pressure and underlying

support, are not possible to measure [Dietrich *et al.*, 1995] or continuously measure in the entire study area [Koukis and Ziourkas, 1991]. Ercanoglu and Gokceoglu [2004] concluded that deterministic approaches can only be used for the small and relatively homogeneous areas and require detailed geotechnical and hydro-geological data. To provide an operational model of landslide susceptibility and hazard analysis, in this research, we employ the probabilistic approach to develop a landslide analysis system (LAS).

Based on the concept describes in [Fourniadis *et al.*, 2007], we propose six strategies to develop the LAS, with the intention to provide more accurate calculations of landslide susceptibility index (LSI) and landslide hazard index (LHI). Each strategy is explained in details in section 2. With this new LAS, we revisit the event of debris flow occurred in He-Jung Village in 2012, and use the archive of QPESUM data to make a series of three-hour nowcasts. Comparing the LHI calculated by LAS to the actual sites of new landslides triggered in this event, the accuracy is as high as 70%. The possible sources of error and the room of further improvement are discussed. The future plan to provide nationwide nowcasts of landslide using this new LAS is also included.

2. LANDSLIDE ANALYSIS SYSTEM

Based on the probabilistic approach of landslide analysis, the development of our LAS is comprised of six steps: prepare landslide inventory, select preparatory factors, establish a model of LSI, determine the weight of each preparatory factor, calculate LHI using triggering factor, and evaluate the performance of model with actual events of landslide. To facilitate the explanation of each step and focus on our target area, only the results of He-Jung Village are presented in this paper. As aforementioned, four basic geospatial data of He-Jung Village are given in Fig. 1 for illustration.

2.1 Long-term and detailed inventory of landslide

Metternicht *et al.* [2005] pointed out that the availability of high spatial resolution satellite imagery presents the opportunity to produce landslide inventory maps. Ostir *et al.* [2003] suggested that an ideal satellite system for monitoring hazards should be able to operate at a continuous monitoring mode, to guarantee that the 'before' pictures are available, and a rapid-response mode, to allow the acquisition of the 'after' pictures shortly after any event of interest.

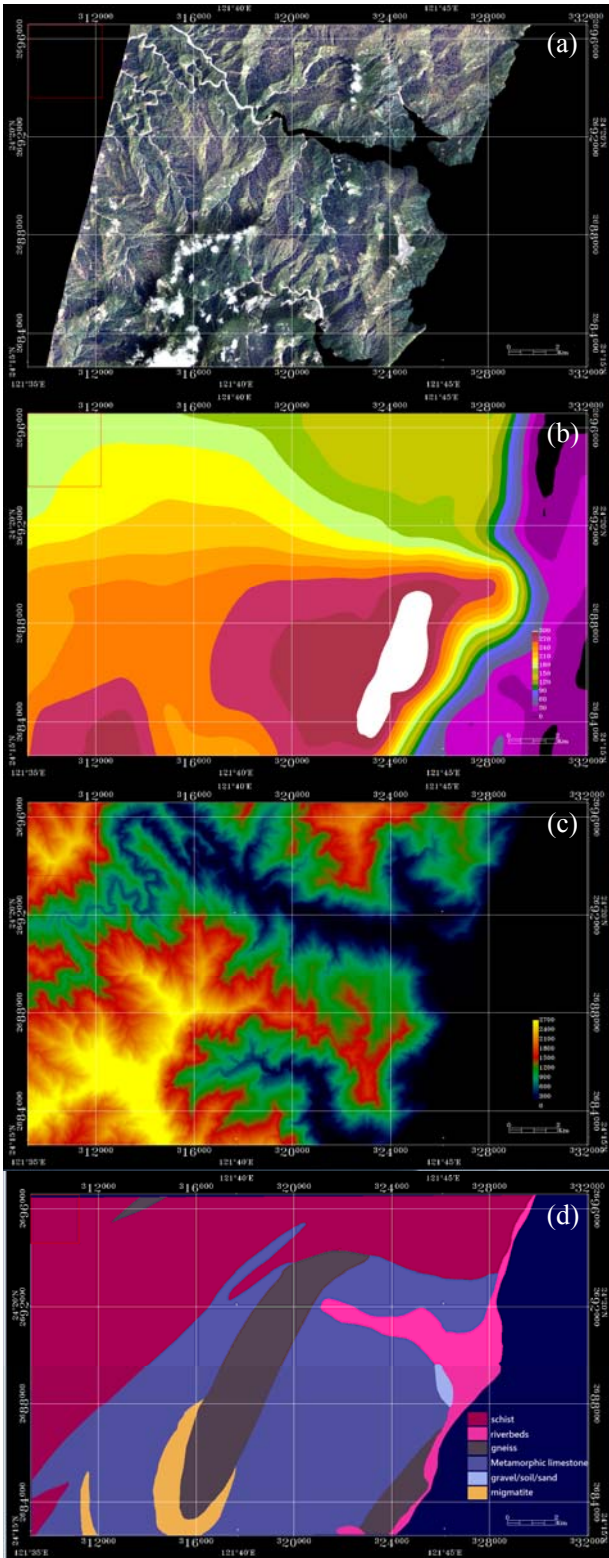


Fig. 1 Examples of four basic geospatial data of He-Jung Village: (a) Formosat-2 image taken on 18 March 2013, (b) QPESUM product of three-hour maximum precipitation from 29 July to 4 August 2013, (c) Digital elevation model with 5m resolution, and (d) geological map (scale: 1/250,000).
 Formosat-2 launched on May 21, 2004 has a unique orbit configuration to enable high spatial resolution imagery acquisition on a daily basis [C-C Liu, 2006]. Formosat-2 has been acquiring more than

25 million km² images of Taiwan area available for 2m in panchromatic (0.45~0.90 μm) and 8m in multispectral (0.45~0.52, 0.52~0.60, 0.63~0.69, 0.76~0.90 μm) with swath of 24 km. Liu *et al.* [2011] demonstrated the potential of Formosat-2 imagery in monitoring the spatial and temporal variations of landslides, especially over Taiwan area.

To prepare a long-term and detailed inventory of landslide in a systematic and consistent way, a three-year project funded by Forestry Bureau was conducted from 2010 to 2012, with focus on employing Formosat-2 imagery to assess and interpret landslides that occur in Taiwan after natural disaster [Lin *et al.*, 2013]. To support this project, the Expert Landslide and Shaded Area Delineation System (ELSADS) was developed to integrate all useful spatial information to prepare an eight-year inventory of landslide for entire Taiwan area in a quick and accurate fashion, based on the characteristics of Normalized Difference Vegetation Index, Greenness, as well as the first principal component of panchromatic band [C-C Liu, 2014]. Figure 2 shows the graphic user interface of ELSADS and one example of landslide and shaded area delineation.

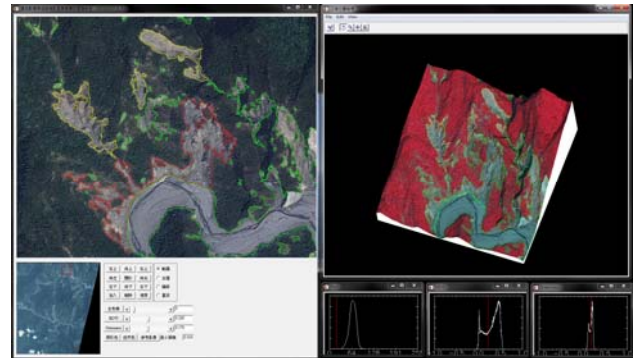


Fig. 2 Graphic user interface of ELSADS

Figure 3 gives the annual inventory of landslide from 2005 to 2012. With this long-term and detailed inventory of landslide, the Soil and Water Conservation Bureau (SWCB) of Taiwan was able to assess the status of 1,664 potential debris flow torrent (PDFT), using the definition of accumulation rate of variation (ARV):

$$ARV \equiv \sum_n |LA_n - LA_{n-1}| / A_{ws} \quad (1)$$

where A_{ws} is the watershed area of PDFT; LA_n and LA_{n-1} are landslide areas of year n and $n-1$, respectively. Table 1 gives a list of torrents that rank top 30 after the variation analysis. Simply based on the statistics of landslide area changes, this result matches the general impression about those torrents with frequent reports of disasters quite well.

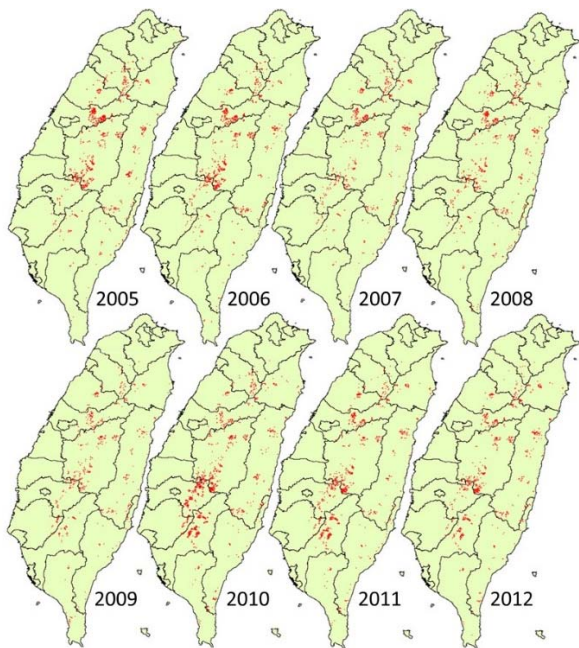


Fig. 3 Annual inventory of landslides from 2005 to 2012.

Table 1 Variation analysis of potential debris flow torrent.

| R | ID. of potential debris flow hazard torrent | Area (Ha) | Rate of landslide area variation (%) | | | | | | | | ARV (%) |
|----|---|-----------|--------------------------------------|-------|-------|-------|-------|-------|-------|--------|---------|
| | | | 2005 | 2006 | 2007 | 2008 | 2009 | 2010 | 2011 | 2012 | |
| 1 | KHC-DF009 | 32.46 | 0.00 | 0.00 | 0.00 | 0.00 | 78.67 | 58.83 | 16.62 | 154.12 | |
| 2 | TCC-DF100 | 16.76 | 16.04 | 8.85 | 37.81 | 2.61 | 0.00 | 29.96 | 3.30 | 98.57 | |
| 3 | TTH-DF068 | 53.96 | 12.03 | 11.04 | 3.43 | 34.53 | 12.77 | 21.46 | 2.17 | 97.43 | |
| 4 | KHC-DF060 | 592.74 | 6.98 | 5.16 | 8.40 | 1.47 | 46.22 | 16.70 | 0.57 | 85.52 | |
| 5 | YLH-DF011 | 17.21 | 0.00 | 0.00 | 0.00 | 20.52 | 12.05 | 32.58 | 2.18 | 67.34 | |
| 6 | CIH-DF056 | 218.29 | 0.07 | 0.00 | 0.00 | 0.00 | 33.36 | 18.69 | 8.75 | 60.88 | |
| 7 | TNH-DF045 | 149.04 | 1.48 | 5.23 | 0.38 | 0.30 | 19.42 | 18.71 | 6.84 | 52.37 | |
| 8 | CIH-DF042 | 115.25 | 1.82 | 0.45 | 0.18 | 0.53 | 34.88 | 1.96 | 10.44 | 50.26 | |
| 9 | TCC-DF034 | 46.44 | 8.92 | 6.20 | 10.68 | 4.18 | 1.08 | 9.84 | 5.26 | 46.17 | |
| 10 | TNH-DF046 | 39.87 | 6.12 | 6.66 | 1.10 | 0.00 | 14.94 | 13.98 | 2.89 | 45.68 | |
| 11 | NTC-DF226 | 408.30 | 0.13 | 5.81 | 6.68 | 0.29 | 24.69 | 3.33 | 4.59 | 45.52 | |
| 12 | CIH-DF048 | 4.76 | 0.00 | 0.00 | 0.00 | 0.00 | 20.60 | 20.60 | 0.00 | 41.20 | |
| 13 | CIH-DF018 | 127.68 | 0.09 | 3.90 | 9.99 | 9.07 | 4.80 | 4.70 | 3.49 | 36.04 | |
| 14 | CIH-DF027 | 64.74 | 4.94 | 1.34 | 2.02 | 3.68 | 7.58 | 8.84 | 4.72 | 33.12 | |
| 15 | TNH-DF001 | 51.50 | 0.61 | 1.34 | 2.47 | 4.59 | 11.50 | 10.34 | 1.92 | 32.78 | |
| 16 | HLH-DF024 | 573.41 | 3.63 | 4.05 | 9.49 | 5.03 | 0.23 | 3.04 | 5.99 | 31.47 | |
| 17 | KHC-DF017 | 6.49 | 0.00 | 0.00 | 0.00 | 0.00 | 15.58 | 7.88 | 7.70 | 31.16 | |
| 18 | NTC-DF196 | 326.08 | 5.66 | 7.86 | 3.29 | 1.29 | 7.30 | 3.73 | 1.83 | 30.96 | |
| 19 | KHC-DF107 | 12.52 | 0.00 | 0.00 | 0.00 | 0.00 | 0.00 | 17.26 | 11.30 | 28.56 | |
| 20 | NTC-DF213 | 41.52 | 1.99 | 1.99 | 0.51 | 0.51 | 11.08 | 7.63 | 3.45 | 27.15 | |
| 21 | KHC-DF078 | 46.13 | 0.00 | 0.00 | 0.00 | 0.00 | 16.12 | 3.36 | 7.62 | 27.11 | |
| 22 | KHC-DF077 | 559.72 | 2.67 | 1.30 | 0.13 | 0.27 | 12.34 | 2.46 | 6.78 | 25.95 | |
| 23 | KHC-DF010 | 77.07 | 0.00 | 0.00 | 0.62 | 0.62 | 11.80 | 10.11 | 1.56 | 24.69 | |
| 24 | KHC-DF102 | 9.54 | 0.00 | 0.00 | 0.00 | 0.00 | 18.05 | 6.02 | 24.07 | | |
| 25 | KHC-DF064 | 299.15 | 0.11 | 0.11 | 0.23 | 1.33 | 13.87 | 5.75 | 2.35 | 23.74 | |
| 26 | KHC-DF055 | 93.13 | 0.00 | 0.00 | 0.00 | 0.00 | 10.62 | 4.27 | 7.55 | 22.45 | |
| 27 | CIH-DF060 | 81.07 | 0.00 | 0.00 | 0.00 | 0.00 | 12.62 | 4.61 | 4.90 | 22.13 | |
| 28 | TCC-DF035 | 50.45 | 5.72 | 1.86 | 5.19 | 1.60 | 0.12 | 2.94 | 4.38 | 21.82 | |
| 29 | CIH-DF051 | 241.10 | 1.05 | 0.40 | 0.13 | 0.15 | 9.55 | 7.96 | 1.54 | 20.77 | |
| 30 | KHC-DF072 | 270.76 | 0.04 | 0.04 | 0.00 | 0.55 | 11.06 | 1.82 | 7.07 | 20.58 | |

R: rank; ARV: accumulation rate of variation.

Table 2 Manifestation of landslides

[summarized from Koukis and Ziourkas, 1991].

| A. Factors contributing to increased shear stress | |
|---|--|
| Transitory earth stresses | Earthquakes |
| | Vibrations from machinery |
| | Vibrations from traffic |
| | Adjacent slope failures |
| Squeezing out of underlying plastic material | |
| Removal of lateral and underlying support | Stream and rivers |
| | Waves |
| | Tidal currents |
| | Precipitation (rain, sleet, snow or hail) |
| | Sub-aerial weathering, wetting and drying and frost action |
| Solution and removal of material | |
| Creation of new slopes | Previous movements |
| | Large scale faulting |
| Work of human agencies | Cuts, pits, etc. |
| | Removal of retaining technical works |
| | Creation of lakes |
| Creation of reservoirs | |
| Natural agencies | Weight of rain, hail, snow and water from springs |
| | Accumulation of talus |
| Vegetation | |
| Surcharge | Fills |
| | Stockpiles of ore |
| | Stockpiles of rock |
| | Stockpiles of rubbish heap |
| | Buildings and other structures |
| | Weight of water from leaking pipe lines, etc. |
| Cultivation and irrigation of slopes | |
| Increase of the slope angle through regional tilting local raising | |
| Volcanic processes | |
| Lateral pressure | Water in cracks and caverns |
| | Freezing of water in cracks |
| | Swelling of clay or anhydrite |
| | Mobilization of residual stress |
| B. Factors contributing to low or reduced shear strength | |
| Changes due to weathering and other physico-chemical reactions | Softening of fissured clays |
| | Physical disintegration of granular rocks |
| | Hydration of clay minerals |
| | Base exchange in clays |
| Drying of shale | |
| Migration of water to weathering front under electrical potential | |
| Initial state | Composition |
| | Texture |
| Gross structure and slope geometry | Fractures |
| | Faults |
| | Bedding planes |
| | Cleavage |
| | Brecciated zones |
| | Massive beds over weak or plastic materials |
| Alternation of permeable and impermeable beds | |
| Slope orientation | |
| Changes of inter-granular forces due to water content and pressure in pores and fractures | Rainfalls |
| | Snowmelt |
| | Diversion of streams |
| | Ponds |
| | Reservoirs |
| Irrigation | |
| Clearing of vegetation and deforestation | |
| Changes in structure | |
| Weakening due to progressive creep | |
| Action of tree roots | |
| Action of burrowing animals | |

2.2 Evaluating and selecting preparatory factors

Koukis and Ziourkas [1991] made a comprehensive review and discussion of various preparatory factors that were used for landslide analysis, as listed in Table 2.

Generally speaking, more than 64 factors had ever been used by various models of LSI. Some of them are not independent, some of them are not possible to be quantified as a parameter, while some of them are not available everywhere. To develop an operational and universal model of landslide susceptibility, Liu *et al.* [2004] suggested that the preparatory factors should be obtainable and applicable to anyplace. Therefore, to develop our

LAS, we started from two topographic properties: slope and aspect, which can be derived from DEM, and one geological property: geological composition, which can be obtained from the geological map.

With this long-term and detailed inventory of landslide for Taiwan area, we are able to evaluate and justify each preparatory factor by relating its values with the occurrence of landslides for the past eight years. A number of intervals is specified and the area ratio of each interval AR_i is defined as

$$AR_i \equiv \frac{A_i}{A_t}, \quad (2)$$

where A_i is the area of interval i , and A_t is the total area of the study area. The weight of each interval W_i is defined as

$$W_i \equiv \frac{L_i}{A_i}, \quad (3)$$

where L_i is the landslide area within interval i . The normalized weight is W_i^* defined as

$$W_i^* \equiv \frac{W_i}{\max(W_i)}, \quad (4)$$

where $\max(W_i)$ is the maximum value of W_i . Figure 4 gives AR_i (green bars) and W_i^* (red bars) for each preparatory factor, including (a) slope, (b) aspect, and (c) geological composition. Note that a large number of intervals is specified to ensure a narrow range of each interval (every one degree for slope and every four degrees for aspect). This would increase the resolution and avoid the ambiguity raised by averaging the contribution over a broader range in one single interval.

AR_i (green bars) in Fig. 4a shows a clear pattern of normal distribution with a peak at about 36° and two troughs towards two ends of high and low slopes. The corresponding W_i^* (red bars) increases monotonically as the slope increases from 20° to 78° , which indicates that slope is highly correlated with landslide. Therefore, slope should be selected as a preparatory factor. Likewise, AR_i (green bars) in Fig. 4b shows a clear pattern with higher values between 270° and 360° (north-west direction), while the corresponding W_i^* (red bars) is comparatively low within this range. This phenomenon reflects the prevailing direction of monsoon: landslides tend to occur facing south-east directions ($90^\circ - 180^\circ$) and more regions with that aspects were collapsed and removed. Since aspect is also highly correlated with landslide, it should be selected as a preparatory factor as well. Geological composition is a nominal property rather than a continuous value. There are six major types of geological composition in He-Jung Village, including schist, gneiss, migmatite, metamorphic limestone, gravel/soil/sand, and

riverbeds. Fig. 4c shows that landslides tend to occur at those regions of gravel and migmatite. Note that the boundaries of various geological compositions are apparently rather rough, as illustrated in Fig. 1d. Without a higher-resolution map of geological composition for He-Jung Village, we have to live with the existing map and bear this in mind to discuss the possible error that might be raised for susceptibility and hazard analysis.

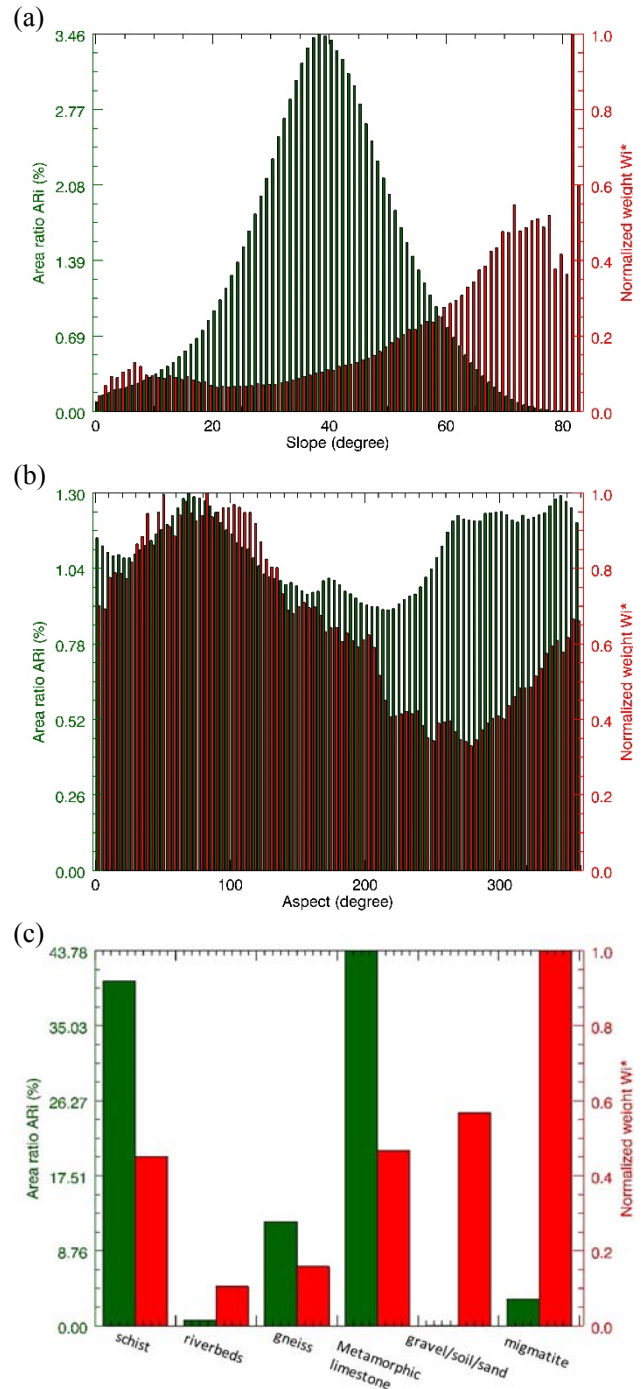


Fig. 4 AR_i (green bars) and W_i^* (red bars) for preparatory factors (a) slope, (b) aspect, and (c) geological composition.

2.3 Total Flux

Most of the preparatory factors proposed and employed by various researchers in the past are pixel-based properties, which can only represent the characteristics of that particular pixel. The occurrence of landslide at one pixel, however, would be effected by the properties of other pixels surrounding that particular pixel as well. For example, even with the same slope, aspect or geological composition, different levels of runoff flushed from the adjacent pixels due to topographic changes should have different effects on landslide susceptibility. This mechanism needs to be included in the model of landslide susceptibility by introducing a region-based preparatory factor.

Quinn *et al.* [2010] introduced the flow accumulation (FA) as a region-based preparatory factor in his model of landslide susceptibility to address this kind of contiguous effect. They calculated FA by the number of map pixels that would direct overland flow to any specific point in the interpreted drainage system. To facilitate the computation, they used different sizes of buffer zones along the river to represent different number of pixels, and landslide incidence is compared with FA in the nearest river within the GIS. At least two assumptions, however, are implicated by use of FA. Firstly, the main stream is determined by connecting the flow directions calculated at each pixel. All runoff at one pixel are assumed to flow to only one direction determined by the largest difference of elevation between that target pixel and eight surrounding pixels. In reality, runoff does not go to one direction only, especially for the case that the differences of elevation between that target pixel and eight surrounding pixels are not significant. Secondly, all pixels within the same buffer zone would be specified to a same value of FA. It is again not valid since other levels of streams would flow into the main stream along the way. Different values of FA should be specified accordingly.

Liu *et al.* [2014] proposed a new region-based preparatory factor of total flux (TF) to eliminate the aforementioned two assumptions. The total amount of water in a grid (m, n) $W_{m,n}$ is the value of TF for that grid (m, n) , which can be decomposed as the summation of precipitation $P_{m,n}$ from the sky and runoff water $R_{m,n}$ from the adjacent grids

$$W_{m,n} = P_{m,n} + R_{m,n}. \quad (5)$$

This amount of water would be distributed to eight surrounding grids (i, j) at a fraction of $F_{m,n \rightarrow i,j}$ based on the topography and hydrology conditions in the vicinity of each grid

$$R_{m,n \rightarrow i,j} = W_{m,n} \times F_{m,n \rightarrow i,j}, \quad (6)$$

where $F_{m,n \rightarrow i,j}$ is proportional to the gradient $G_{m,n \rightarrow i,j}$.

$$F_{m,n \rightarrow i,j} \equiv \frac{G_{m,n \rightarrow i,j}}{\sum G_{m,n \rightarrow i,j}}, \quad (7)$$

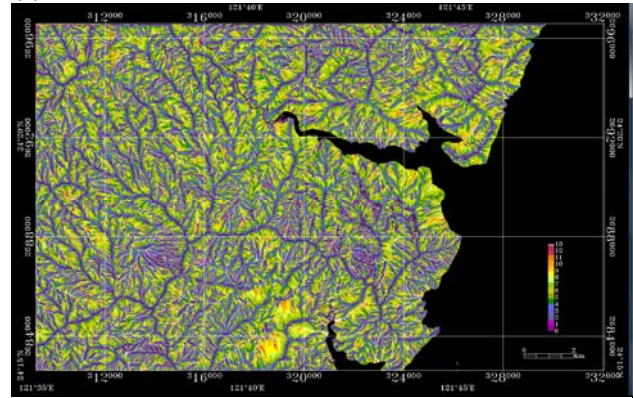
$$G_{m,n \rightarrow i,j} \equiv \frac{H_{m,n} - H_{i,j}}{D_{m,n \rightarrow i,j}} \text{ where } \begin{matrix} i = m-1, m, m+1 \\ j = n-1, n, n+1 \end{matrix} \quad (8)$$

$H_{m,n}$ and $H_{i,j}$ are elevations at pixel (m, n) and pixel (i, j) , respectively. $D_{m,n \rightarrow i,j}$ is the distance between pixel (m, n) and pixel (i, j) .

$$D_{m,n \rightarrow i,j} = \begin{cases} 1 & \text{if } i = m \text{ or } j = n \\ \sqrt{2} & \text{if } i \neq m \text{ and } j \neq n \end{cases} \quad (9)$$

Note that the calculation is started from the pixel with the highest elevation and then move the pixels with the second highest elevation, etc., to ensure $H_{m,n}$ is no less than $H_{i,j}$ and $G_{m,n \rightarrow i,j}$ is not a negative value.

(a)



(b)

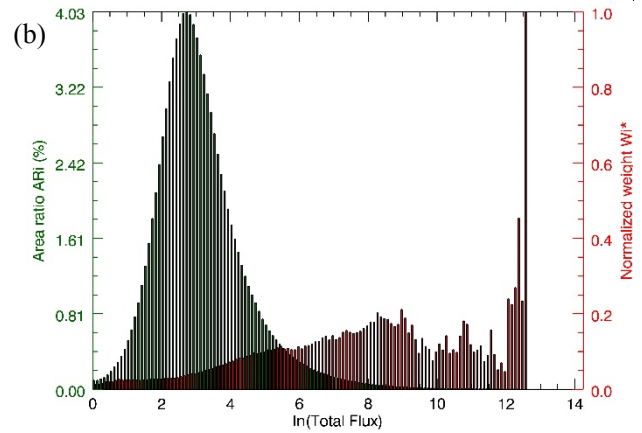


Fig. 5 (a) map of TF of He-Jung Village derived from DEM (Fig. 1c) using Eq. (5) – (9). (b) The corresponding AR_i (green bars) and W_i^* (red bars) as a function of $\ln(TF)$.

Figure 5a shows the map of TF of He-Jung Village derived from DEM (Fig. 1c) using Eq. (5) – (9). The network shown in blue color matches the ridgeline very well, because all waters in this region are basically from sky only. They are distributed immediately to the adjacent pixels. By contrast, the regions shown in yellow or red colors are the pixels where waters are flushed into or passed by. They

certainly would have a higher susceptibility of landslide, yet they don't have to be within the main stream. AR_i (green bars) in Fig. 5b shows a pattern of Gaussian distribution with a peak at about $e^{2.7}$ and two troughs towards two ends of high and low slopes. The corresponding W_i^* (red bars) shows another pattern of Gaussian distribution with a peak at about $e^{8.3}$, which indicates that TF is highly correlated with landslide. Therefore, TF serves as an ideal preparatory factor.

2.4 Optimizing the relative contribution

With all preparatory factors available, the general approach to evaluate the susceptibility of landslide is to calculate the arithmetic or geometric means of all preparatory factors, under the assumption that all preparatory factors are equally weighted, such as the works by [J G Liu et al., 2004; Nguyen and Liu, 2014]. The expert grading method is another way to specify the weighting value for each individual factor, which however, is inevitably biased by the subjective grading system of different expert [Stevenson, 1977]. Since the long-term and detailed inventory of landslide for Taiwan area is available, we are able to employ various techniques of optimization to derive the relative contribution for each factor. Before doing that, we need a quantitative way to evaluate the performance of various models of landslide susceptibility.

Oh and Lee [2011] proposed to use a cumulative percentage of landslide occurrence to validate various susceptibility models of landslide. But there is no explicit definition of threshold that can be used, from the operational point of view. We follow the similar concept and calculate two cumulative probability of landslide occurrence for both the actual landslide areas and non-landslide areas, respectively. The threshold is selected to maximize both the number of predicted landslide areas within the actual landslide areas (positive right) and the number of predicted non-landslide areas within the actual non-landslide areas (negative right), as well as minimize the number of predicted non-landslide areas within the actual landslide areas (missing) and the number of predicted landslide areas within the actual non-landslide areas (false alarm), as illustrated by the annotation in Fig. 6a. We started from the deterministic arithmetic model (Fig. 6a):

$$LSI_{DA} = (W_{Slope}^* + W_{Aspect}^* + W_{TF}^* + W_{GC}^*)/4, \quad (10)$$

and the deterministic geometric model (Fig. 6b):

$$LSI_{DG} = (W_{Slope}^* \times W_{Aspect}^* \times W_{TF}^* \times W_{GC}^*)^{1/4}, \quad (11)$$

where the threshold and model performance are given in Table 3 for comparison.

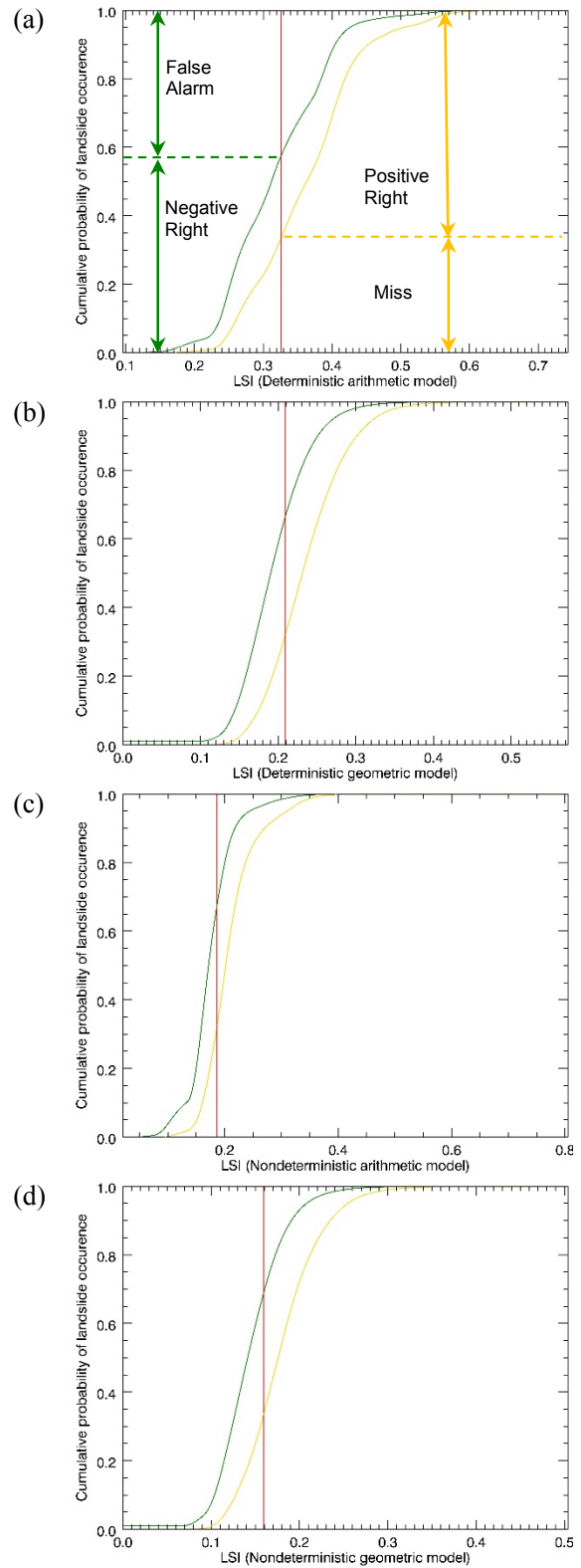


Fig. 6 Cumulative probability of landslide occurrence for both the actual landslide areas (yellow curve) and non-landslide areas (green curve), respectively. Threshold (red line) is determined by maximizing the sum of positive right and negative right, as well as minimizing the sum of missing and false alarm. (a) Deterministic arithmetic model, (b) Deterministic geometric model, (c) Nondeterministic arithmetic model, (d) Nondeterministic geometric model.

Table 3 Quantitative assessment of four models of *LSI*.

| | DA | DG | NDA | NDG |
|--------------------|-------|-------|-------|-------|
| Threshold | 0.33 | 0.21 | 0.19 | 0.16 |
| Positive Right (%) | 66.69 | 68.01 | 68.18 | 66.68 |
| Negative Right (%) | 57.37 | 66.49 | 67.15 | 68.75 |
| Miss (%) | 33.31 | 31.99 | 31.82 | 33.32 |
| False Alarm (%) | 42.63 | 33.51 | 32.86 | 31.25 |

We took a further step to employ the downhill simplex method [Nelder and Mead, 1965] to search the optimized value of relative contribution for each factor, resulting in the nondeterministic arithmetic model

$$LSI_{NDA} = 0.27 \times W_{Slope}^* + 0.03 \times W_{Aspect}^* + 0.65 \times W_{TF}^* + 0.21 \times W_{GC}^*, \quad (12)$$

and the nondeterministic geometric model

$$LSI_{NDG} = W_{Slope}^{*0.3} \times W_{Aspect}^{*0.15} \times W_{TF}^{*0.31} \times W_{GC}^{*0.31}. \quad (13)$$

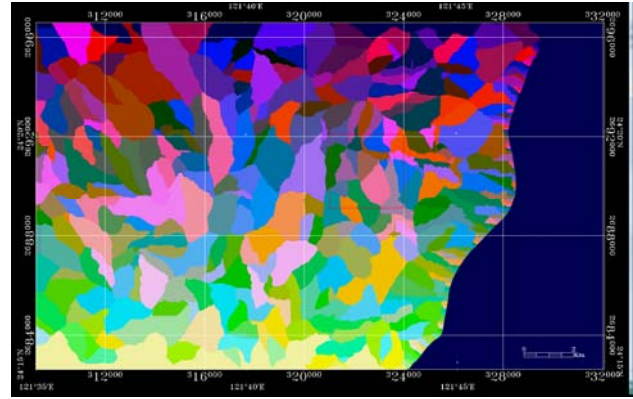
Generally speaking, deterministic geometric model (Eq. 11) performs better than deterministic arithmetic model (Eq. 10), while optimizing the relative contribution for each factor makes no significant improvement, either the case of nondeterministic arithmetic model (Eq. 12) or the case of nondeterministic geometric model (Eq. 13), as compared in Table 3.

2.5 The smallest watershed

Up to now, the best accuracy of four models of *LSI* is only about 67%. After carefully examining those pixels with wrong predictions, we realize that there are still some landslides occurred at those pixels with low value of *LSI*. These pixels are supposed to be stable, but some of their contiguous pixels are collapsed. This kind of contiguous effects, however, cannot be addressed by computing *LSI* at pixel scale. Therefore, we introduce the concept of the smallest watershed and treat all pixels within the same watershed as an entity, namely group unit *GU*. The smallest watershed is defined as the minimum area of watershed, as the number of landslide areas reaches its maximum number within the specified watershed.

Figure 7 gives the map of *GU* of He-Jung Village. We repeat the same procedures as described in section 2.4 to evaluate four models of *LSI*. But the highest value of *LSI* within the same *GU* would be used to represent the *LSI* of that particular *GU*. The quantitative results are given in Table 4. The accuracy is indeed much improved from 67% to approximately 78%. This also suggests that a better way to employ this kind of *LSI* model is to make

prediction and send alarms at the scale of the smallest watershed.

**Fig. 7** Map of *GU* of He-Jung Village.**Table 4** Quantitative assessment of four models of *LSI* by considering the smallest watershed (*GU*-based analysis).

| | GDA | DGD | GNDA | GNDG |
|--------------------|-------|-------|-------|-------|
| Threshold | 0.46 | 0.29 | 0.27 | 0.25 |
| Positive Right (%) | 68.57 | 85.31 | 83.67 | 75.10 |
| Negative Right (%) | 86.84 | 71.05 | 73.03 | 80.26 |
| Miss (%) | 31.43 | 14.69 | 16.33 | 24.90 |
| False Alarm (%) | 13.16 | 28.95 | 26.97 | 19.74 |

2.6 Determining the weighting of precipitation

In order to make nowcasts of landslide over the entire country during a typhoon or storm event, the trigger factor of precipitation needs to be incorporated with *LSI* to calculate *LHI*. As aforementioned, QPESUMS provides real-time estimation and up to 72 hours forecast of nationwide precipitation, and the data are updated every ten minutes at a spatial resolution of 1.3km. It is an ideal data source of triggering factor for landslide analysis. To quantitatively describe the relationship between *LHI*, *LSI* and the precipitation *R*, we define

$$LHI \equiv LSI \times R^n, \quad (14)$$

where *n* is the relative contribution of *R* to *LHI*. Lin [2013] tested various products of QPESUMS in Beinan River Drainage of East Taiwan, and concluded that the product of three-hour maximum precipitation $3Hr_{max}$ correlates to *LHI* the best. Three different values of *n* (0.25, 0.33, 0.5) were also attempted, and the results indicated that the value of 0.25 represents *n* quite well. To expand its application to He-Jung Village, we focus on an earlier event of large-scale landslide occurred in Typhoon Megi (20 October 2010). The event-based inventory of landslide and the QPESUMS product of $3Hr_{max}$ (Fig. 1b) are prepared. The downhill simplex method [Nelder and Mead, 1965] is employed again to search an optimized value of *n*. The result indicates that

0.705 is a representative value of n for He-Jung Village, based on optimization analysis of the event-based inventory of landslide and the QPESUMS product of $3Hr_{max}$ (Fig. 1b).

$$LHI \equiv LSI \times 3Hr_{max}^{0.705} \quad (15)$$

With Eq. (15), we revisit the event of debris flow occurred in He-Jung Village triggered by Typhoon Saola in 2012.

3. APPLICATION IN TYPHOON SAOLA

Typhoon Saola struck Taiwan on 2 July 2012 and brought substantial precipitation. The highest total precipitation (1,922 mm) was reported at Tai-Ping station, and the highest hourly precipitation (125 mm) was measured at He-Jung. Extensive floods were triggered consequently. One debris flow hit He-Jung Village and buried several houses instantly. Since this area was not classified as a PDFT before, this catastrophic event raises three major questions: How is this happened? Is there any other place that is at the same risk? What should we do to avoid the similar disasters in the future, from the point of view of management and mitigation? To answer these questions, we attempt to apply our LAS to revisit this event by analysing landslide susceptibility and hazard, as well as using the archive of QPESUM data to make a series of nowcasts. The ultimate goal is to provide early warnings to the general publics to reduce the risk of slope hazards.

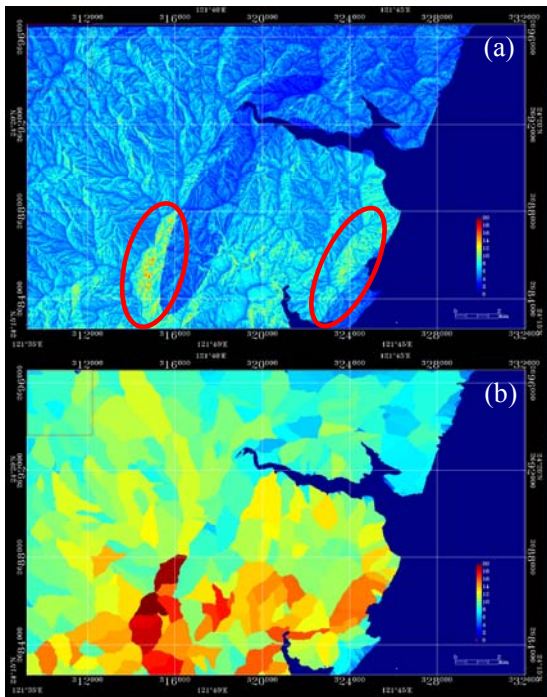


Fig. 8 Map of LHI of He-Jung Village: (a) pixel-based analysis, and (b) GU-based analysis.

Figure 8 shows the map of LHI of He-Jung

Village using pixel-based and GU-based analysis, respectively. Note that the LSI is calculated by the nondeterministic geometric (NDG) model described in section 2.4. A quantitative assessment is given in Table 5. Since the existing geological map of He-Jung Village is at a scale of 1/250,000. There is an artificial boundary between gneiss and migmatite in the lower-middle part of the map. This boundary is not realistic and might be the main source of error. Nevertheless, the accuracy of pixel-based analysis is as high as approximately 65%. The accuracy of GU-based analysis is much improved for positive right (76%), yet is slightly degraded for negative right (62%). To illustrate the matches between the predicted hot spots of landslides and the actual region of landslide, two regions circled in red colour in Fig. 8 are overlaid with landslide layer and displayed on Google Earth, as shown in Fig. 9. This result encourages us to employ this new LAS to provide nationwide nowcasts of landslide, using the pre-calculated LSI and QPESUMS product of $3Hr_{max}$.

Table 5 Quantitative assessment of LHI (NDG model).

| | Pixel-based | GU-Based |
|--------------------|-------------|----------|
| Threshold | 5.58 | 8.50 |
| Positive Right (%) | 65.51 | 76.34 |
| Negative Right (%) | 63.92 | 61.48 |
| Miss (%) | 34.49 | 23.66 |
| False Alarm (%) | 36.08 | 38.52 |

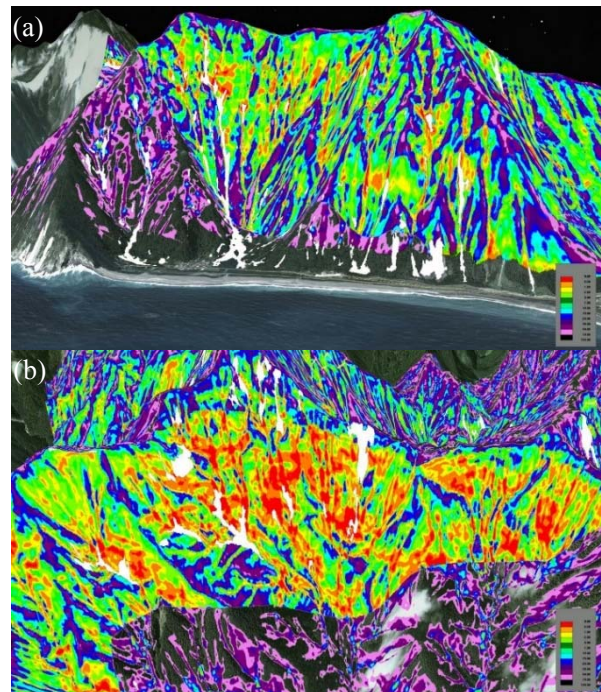


Fig. 9 Illustration of the matches between the predicted hot spots of landslides and the actual region of landslide. (a) He-Jung Village, and (b) the upstream of Shakadang Trail.

4. CONCLUDING REMARKS

Based on the probabilistic approach of landslide analysis, we propose six strategies to develop a LAS, including prepare a long-term and detailed landslide inventory, select preparatory factors, establish a model of LSI, determine the weight of each preparatory factor, calculate landslide hazard index LHI using triggering factor, and evaluate the performance of model with actual events of landslide. With this new LAS, we revisit the event of debris flow occurred in He-Jung Village in 2012, and use the archive of QPESUM data to make a series of three-hour nowcasts. Comparing the LHI calculated by LAS to the actual sites of new landslides triggered in this event, the accuracy is as high as 69%. This result encourages us to employ this new LAS to provide nationwide nowcasts of landslide, using the pre-calculated LSI and QPESUMS product of $3Hr_{max}$.

ACKNOWLEDGMENT: This research is funded by Soil and Water Conservation Bureau, Council of Agriculture, Taiwan, (SWCB-102-071), as well as National Science Council of Taiwan, (NSC 102-2627-B-006-013, NSC 102-2611-M-006-002).

REFERENCES

- Aleotti, P., and R. Chowdhury (1999), Landslide hazard assessment: summary review and new perspectives, *Bull Eng Geol Env*, 58(1), 21-44, doi:10.1007/s100640050066.
- Dietrich, W. E., R. Reiss, M.-L. Hsu, and D. R. Montgomery (1995), A process-based model for colluvial soil depth and shallow landsliding using digital elevation data, *Hydrological Processes*, 9(3-4), 383-400, doi:10.1002/hyp.3360090311.
- Dilley, M., R. S. Chen, U. Deichmann, A. L. Lerner-Lam, M. Arnold, J. Agwe, P. Buys, O. Kjekstad, B. Lyon, and G. Yetman (2005), Natural disaster hotspots: a global risk analysis Rep., 29 pp.
- Domakinis, C., D. Oikonomidis, and T. Astaras (2008), Landslide mapping in the coastal area between the Strymonic Gulf and Kavala (Macedonia, Greece) with the aid of remote sensing and geographical information systems, *International Journal of Remote Sensing*, 29(23), 6893-6915, doi:10.1080/01431160802082130.
- Ercanoglu, M., and C. Gokceoglu (2004), Use of fuzzy relations to produce landslide susceptibility map of a landslide prone area (West Black Sea Region, Turkey), *Engineering Geology*, 75(3-4), 229-250, doi:http://dx.doi.org/10.1016/j.enggeo.2004.06.001.
- Fourmiadis, I. G., J. G. Liu, and P. J. Mason (2007), Regional assessment of landslide impact in the Three Gorges area, China, using ASTER data: Wushan-Zigui, *Landslides*, 4(3), 267-278, doi:10.1007/s10346-007-0080-5.
- Huang, J. C., S. J. Kao, M. L. Hsu, and Y. A. Liu (2007), Influence of Specific Contributing Area algorithms on slope failure prediction in landslide modeling, *Nat. Hazards Earth Syst. Sci.*, 7(6), 781-792, doi:10.5194/nhess-7-781-2007.
- Koukis, G., and C. Ziourkas (1991), Slope instability phenomena in Greece: A statistical analysis, *Bulletin of the International Association of Engineering Geology*, 43(1), 47-60, doi:10.1007/BF02590170.
- Lin, E.-J. (2013), Calculating the relative contributions of various factors in a landslide susceptibility model based on earthquake and typhoon events – an example of Beinan River Drainage, M.Sc. thesis, 127 pp, National Cheng Kung University, Tainan.
- Lin, E.-J., C.-C. Liu, C.-H. Chang, I.-F. Cheng, and M.-H. Ko (2013), Using the FORMOSAT-2 high spatial and temporal resolution multispectral image for analysis and interpretation landslide disasters in Taiwan, *Journal of Photogrammetry and Remote Sensing*, 17(1), 31-51.
- Liu, C.-C. (2006), Processing of FORMOSAT-2 daily revisit imagery for site surveillance, *IEEE Transactions on Geoscience and Remote Sensing*, 44(11), 3206-3214.
- Liu, C.-C. (2014), A fast and accurate approach to prepare a landslide and shadow inventory map from high-spatial-resolution imagery, submitted.
- Liu, C.-C., W. Luo, M.-C. Chen, Y.-T. Lin, K.-w. Yen, H.-L. Wen, and H.-Y. Yin (2014), A region-based factor of total flux for modeling the susceptibility of landslide, in preparation.
- Liu, C.-C., C.-L. Shieh, J.-C. Lin, and A.-M. Wu (2011), Classification of non-vegetated areas using Formosat-2 high spatiotemporal imagery: the case of Tseng-Wen Reservoir catchment area (Taiwan), *International Journal of Remote Sensing*, 32(23), 8519-8540, doi:10.1080/01431161.2010.542200.
- Liu, J. G., P. J. Mason, N. Clerici, S. Chen, A. Davis, F. Miao, H. Deng, and L. Liang (2004), Landslide hazard assessment in the Three Gorges area of the Yangtze river using ASTER imagery: Zigui-Badong, *Geomorphology*, 61(1-2), 171-187, doi:10.1016/j.geomorph.2003.12.004.
- Metternicht, G., L. Hurni, and R. Gogu (2005), Remote sensing of landslides: An analysis of the potential contribution to geo-spatial systems for hazard assessment in mountainous environments, *Remote Sensing of Environment*, 98(2-3), 284-303, doi:10.1016/j.rse.2005.08.004.
- Nelder, J. A., and R. Mead (1965), A Simplex Method for Function Minimization, *The Computer Journal*, 7(4), 308-313, doi:10.1093/comjnl/7.4.308.
- Nguyen, T.-T.-N., and C.-C. Liu (2014), Combining bivariate and multivariate statistical analyses to assess landslide susceptibility in the Chen-Yu-Lan watershed, Nantou, Taiwan, *Sustainable Environment Research*, accepted.
- Oh, H.-J., and S. Lee (2011), Cross-application used to validate landslide susceptibility maps using a probabilistic model from Korea, *Environ Earth Sci*, 64(2), 395-409, doi:10.1007/s12665-010-0864-0.
- Ostir, K., T. Veljanovski, T. Podobnikar, and Z. Stancic (2003), Application of satellite remote sensing in natural hazard management: the Mount Mangart landslide case study, *International Journal of Remote Sensing*, 24(20), 3983-4002.
- Quinn, P. E., D. J. Hutchinson, M. S. Diederichs, and R. K. Rowe (2010), Regional-scale landslide susceptibility mapping using the weights of evidence method: an example applied to linear infrastructure, *Canadian Geotechnical Journal*, 47(8), 905-927.
- Stevenson, P. C. (1977), An empirical method for the evaluation of relative landslip risk, *Bulletin of the International Association of Engineering Geology*, 16(1), 69-72, doi:10.1007/BF02591451.